Heliyon 10 (2024) e38318

Contents lists available at ScienceDirect

Heliyon

journal homepage: www.cell.com/heliyon

Research article

Dual-channel fluorescent sensor for rapid Cu^{2+} and Fe^{3+} detection: Enhanced sensitivity and selectivity with triazole-substituted acridinedione derivative

Srinivasan Parthiban Ragavi [a], Dhakshanamurthy Thirumalai [b], Indira Viswambaran Asharani [a,*], Vidya Radhakrishnan [c], Peter Jerome [d]

[a] Department of Chemistry, School of Advanced Sciences, Vellore Institute of Technology, Vellore-632 014, Tamil Nadu, India
[b] Department of Chemistry, Thiruvalluvar University, Vellore-632 115, Tamil Nadu, India
[c] VIT School of Agricultural Innovations and Advanced Learning, Vellore Institute of Technology, Vellore-632 014, Tamil Nadu, India
[d] School of Chemical Engineering, Yeungnam University, Gyeongsan, 38541, Republic of Korea

ARTICLE INFO

Keywords:
Triazole-based acridinedione
Fluorescent sensor (**AR-2**)
Cu^{2+} and Fe^{3+} metal ions
DFT
Test kit

ABSTRACT

The **AR-2** sensor, derived from a triazole-substituted acridinedione, exhibits distinct responses to Cu^{2+} and Fe^{3+} ions. It shows fluorescence enhancement in the presence of Cu^{2+} ions and a reduction in fluorescence with Fe^{3+} ions. This sensor is distinguished by its high sensitivity, selectivity, rapid response time, reversibility, and broad operating pH range, with shallow detection limits for both ions. Structural and photophysical analyses of **AR-2** were conducted using density functional theory (DFT) and various spectroscopic techniques. The binding modes and recognition mechanisms for Cu^{2+} and Fe^{3+} ions were elucidated through multiple experimental approaches. Additionally, **AR-2** demonstrated efficacy in the rapid, visual detection of these ions via paper test strips and swab tests. It successfully identified Cu^{2+} and Fe^{3+} ions in real water and food samples, achieving notable recovery rates. The **AR-2** sensor also excelled in fluorescence imaging, effectively visualizing iron and copper pools in seed sprouts.

1. Introduction

Copper is an essential trace element in human physiology, performing critical functions within the body. However, excessive copper pollution can negatively impact ecosystems and lead to harmful copper accumulation in humans, posing health risks [1]. While Cu^{2+} is crucial for processes such as Adenosine Triphosphate (ATP) production, catecholamine biosynthesis, and protection against oxidative stress [2], disruptions in Cu^{2+} homeostasis can severely threaten cellular integrity. Such imbalances are linked to neurodegenerative disorders, including Menkes [3], Wilson's [4], Alzheimer's [5], Parkinson's [6], and amyotrophic lateral sclerosis (ALS) [7].

Iron also plays a vital role in numerous biological processes, acting as an oxygen carrier and enzyme cofactor [8], and is integral to cellular metabolism as well as DNA and RNA synthesis [9]. Given its essential nature, Fe^{3+} ions are commonly added to various products such as food, medicine, pesticides, and fertilizers to enhance absorption by crops and humans. However, both iron deficiency and excessive accumulation can lead to serious health issues, including cancer, neurodegenerative diseases, and cardiovascular

* Corresponding author.
E-mail address: asharani.iv@vit.ac.in (I.V. Asharani).

https://doi.org/10.1016/j.heliyon.2024.e38318
Received 21 May 2024; Received in revised form 20 August 2024; Accepted 22 September 2024
Available online 24 September 2024

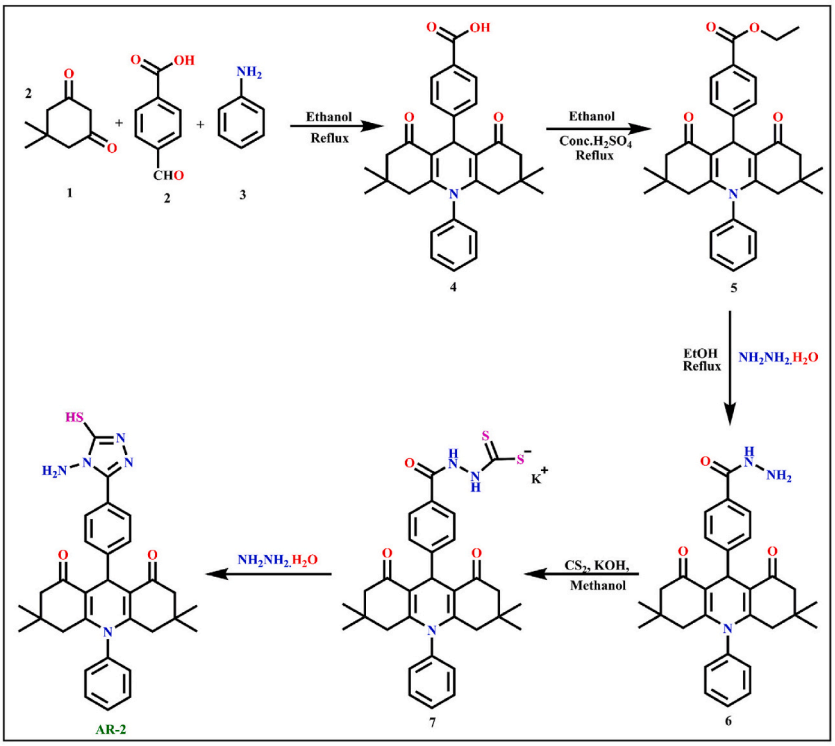

Scheme 1. Synthesis of **AR-2** Probe.

problems. These conditions are closely related to the regulation of iron transport, storage, and balance in the body [10]. Excess iron accumulation can cause organ dysfunction and, in severe cases, be fatal [11]. Consequently, the US Environmental Protection Agency (EPA) recommends limiting daily intake of Cu^{2+} and Fe^{3+} from food and water [12].

Therefore, a straightforward method for simultaneous detection of Cu^{2+} and Fe^{3+} ions is essential. Various systematic methods for detecting these ions exist, including atomic absorption spectrometry (AAS) [13], inductively coupled plasma atomic emission spectrometry (ICP-AES), inductively coupled plasma mass spectrometry (ICP-MS) [14,15], and ion chromatography [16]. However, these techniques often have limitations such as low sensitivity, complex procedures, high costs, and the need for specialized equipment and trained personnel, making them less suitable for real-time monitoring [17].

Fluorescent sensors are currently attracting significant interest due to their numerous advantages, including high selectivity, exceptional sensitivity, ease of use, cost-effectiveness, quantifiability, rapid response, and suitability for real-time and in-situ monitoring [18]. These benefits have spurred researchers to actively develop innovative fluorescent sensors with enhanced sensitivity and selectivity for detecting various substances [19]. There is growing attention towards the development of fluorescence sensors capable of simultaneously identifying multiple metal ions [20]. Several sensors have been designed specifically to detect Cu^{2+} and Fe^{3+} ions with high sensitivity and selectivity [21–25]. However, some sensors designed for detecting Fe^{3+} or Cu^{2+} exhibit limitations such as irreversible response [26], slow reaction times [27], and susceptibility to interference from other metal ions [28]. Moreover, there is a notable lack of colorimetric and fluorescent sensors capable of simultaneously detecting both Cu^{2+} and Fe^{3+} ions [29,30]. Therefore, there is a crucial need to develop straightforward and efficient dual-function colorimetric and fluorescent sensors that can rapidly and selectively detect both Cu^{2+} and Fe^{3+} ions while offering good reversibility.

Acridinedione is a popular choice for fluorescent probes due to its capacity to produce strong and tunable fluorescence, making it valuable for a variety of molecular sensing and imaging applications. Its favorable photophysical properties and versatility are key factors driving the development of these probes. In this study, we introduce **AR-2** (9-(4-(4-amino-5-mercapto-4H-1,2,4-triazol-3-yl) phenyl)-3,3,6,6-tetramethyl-10-phenyl-3,4,6,7,9,10-hexahydroacridine-1,8(2H, 5H)-dione), a novel fluorescent probe derived from acridinedione with a triazole group substitution. **AR-2** exhibits highly selective fluorescence enhancement in response to Cu^{2+} ions and specific fluorescence quenching when exposed to Fe^{3+} ions, compared to other metal ions, across a broad pH range. The recognition of Cu^{2+} and Fe^{3+} is rapidly reversible, occurring within a minute. **AR-2** also demonstrates exceptionally low limits of detection for Cu^{2+} and Fe^{3+}, at 0.883×10^{-7} M and 1.05×10^{-7} M, respectively. We thoroughly investigate the binding modes and recognition mechanisms for Cu^{2+} and Fe^{3+}. Additionally, we develop test strips using the triazole-substituted acridinedione (**AR-2**) with a UV light indicator for the detection of Cu^{2+} and Fe^{3+}.

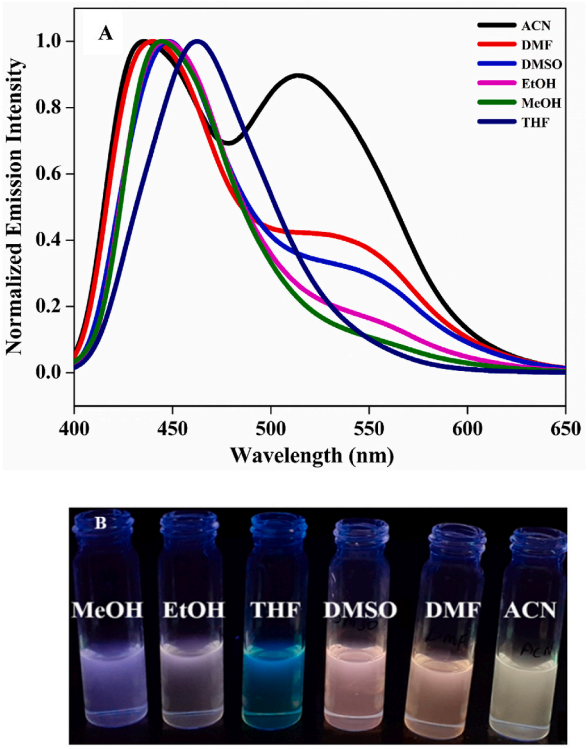

Fig. 1. The solvatochromic effect of the **AR-2** probe (A) on emission spectra in various solvents and (B) Under a UV chamber.

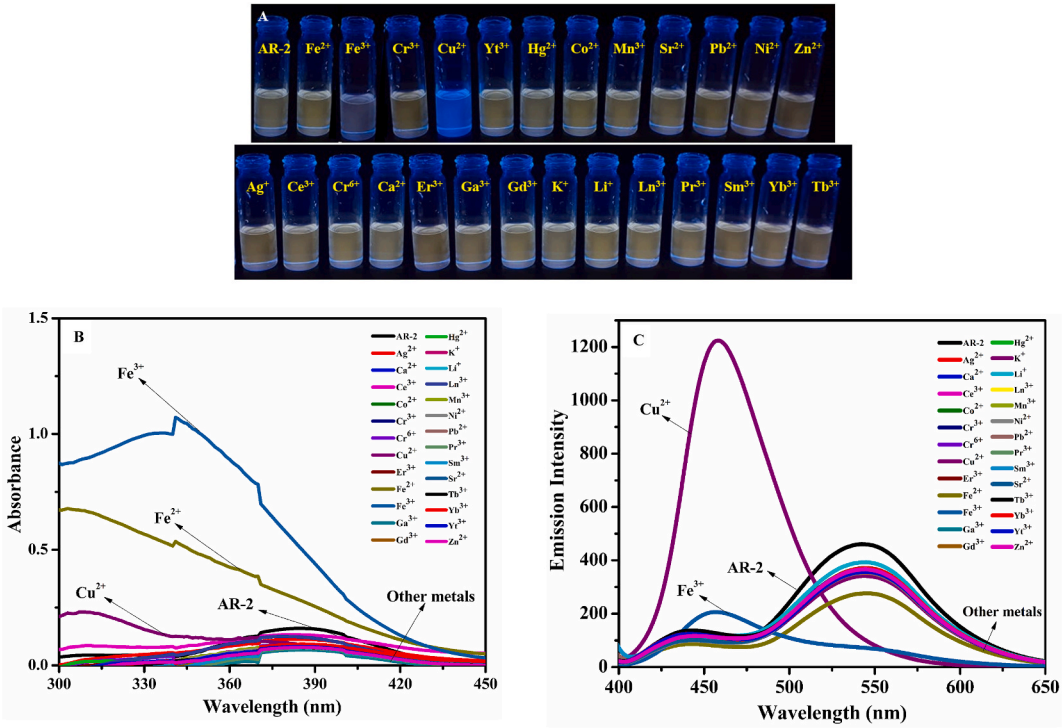

Fig. 2. (A) Visual observation of the color change upon the addition of various metal ions to the **AR-2** probe under a UV lamp, (B) Selectivity of the **AR-2** probe towards Cu^{2+} and Fe^{3+} ions compared to other cations using the UV–visible spectrophotometer and (C) Fluorescence spectral response of the **AR-2** probe towards various cations in a DMSO medium.

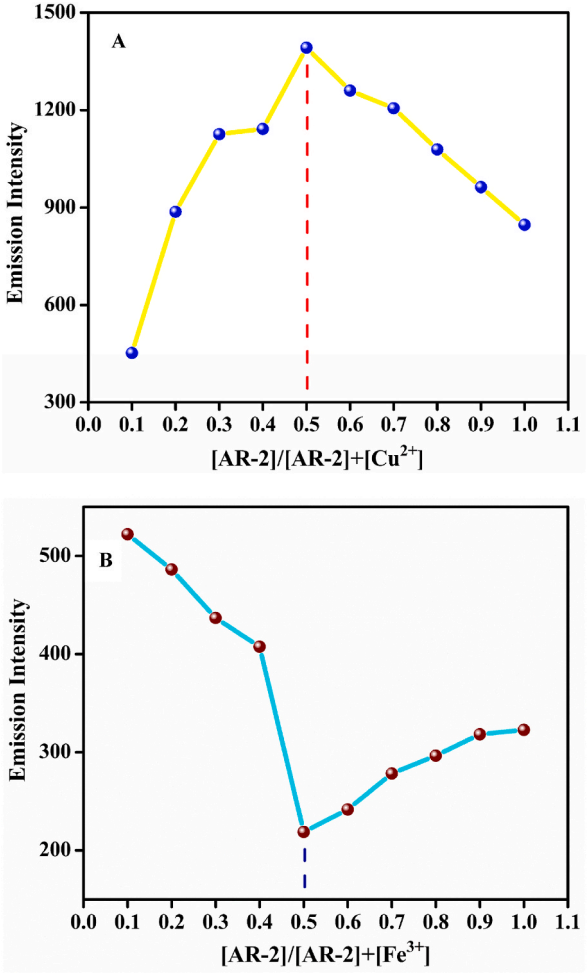

Fig. 3. (A) Job's plot of **AR-2**/Cu^{2+} and (B) Job's plot of **AR-2**/Fe^{3+}.

2. Experiment section

2.1. Materials and instruments

Dimedone, carbon disulfide, hydrazine hydrate, aniline, potassium hydroxide, 4-formyl benzoic acid, ethanol, dimethyl sulfoxide, and various metal salts were obtained from several suppliers, including TCI Chemicals, Avra, Sigma-Aldrich, and Sd-fine Ltd. Deionized water was used exclusively throughout the experiment. Analytical-grade solvents were employed for synthesis, development, extraction, and analysis, obviating the need for further purification. The product was monitored using thin-layer chromatography (TLC), with detection under UV and fluorescent lamps. Purification of the product was carried out using column chromatography with silica gel (60–120 mesh).

The ^{1}H and ^{13}C NMR spectra were obtained utilizing an Advance Bruker spectrometer, operating at 400 MHz for ^{1}H NMR and 100 MHz for ^{13}C NMR in DMSO-d_6 and $CDCl_3$, respectively. Chemical shift values are reported in δ (parts per million). Infrared spectra, covering the 4000-400 cm^{-1} range, were obtained using the KBr pellet technique on a Shimadzu FT-IR spectrometer. High-resolution mass spectra (HRMS) were acquired with the WATER-XEVO G2XS-QT spectrometer. UV absorption spectra were measured with the Agilent 8543 Ultraviolet–Visible spectrophotometer. Finally, fluorescence measurements were performed at room temperature using an Edinburgh FLS 980 fluorescence spectrophotometer, with a scan rate of 1200 nm/min.

2.2. Synthesis of the probe *AR-2*

The synthesis of the triazole-substituted acridinedione compound (**AR-2**) involves five steps, as outlined in Scheme 1. Detailed characterization and the complete synthesis procedure are provided in the supporting information (Figs. S1–S12).

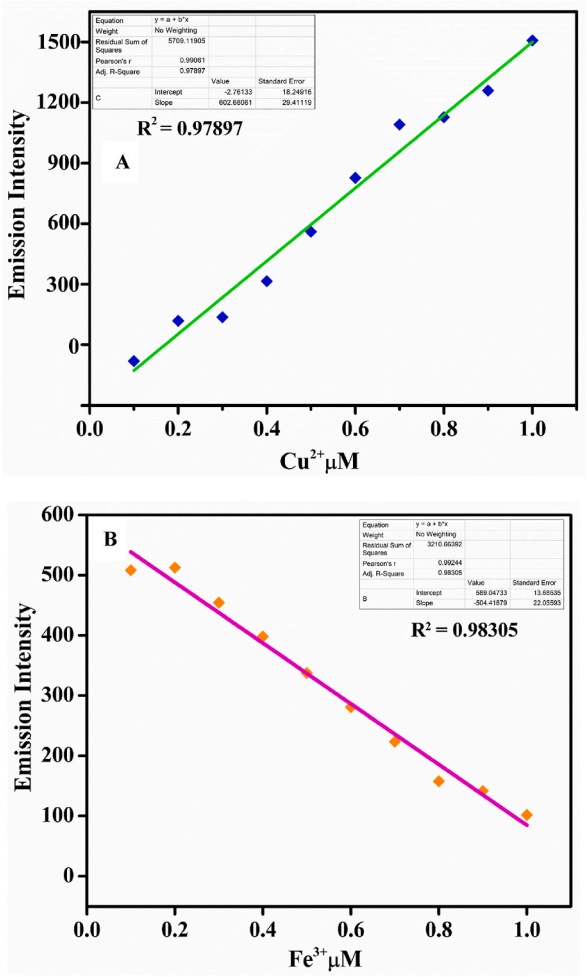

Fig. 4. (A) Titration plot of **AR-2**/Cu^{2+} and (B) Titration plot of **AR-2**/Fe^{3+}.

3. Results and discussion

3.1. Solvent-dependent photophysical studies

The **AR-2** probe was examined in various solvents to understand its behavior across different polarities. UV–visible and fluorescence spectra were recorded to evaluate its intramolecular charge transfer (ICT) potential. Solvents with a range of polarities, from low to high, were tested. Visual observations under a UV lamp (Fig. 1B), as well as absorption and emission spectra (Fig. 1A), were collected. It was observed that the **AR-2** probe had poor solubility in methanol, ethanol, acetonitrile, and DMF, while it dissolved well in DMSO and THF. Due to the low toxicity of DMSO, it was chosen to assess the efficacy of the probe's ICT behavior.

3.2. Selectivity of *AR-2* probe

The **AR-2** probe, at a concentration of 2×10^{-5} M, was tested in both DMSO and aqueous solutions for absorbance and fluorescence measurements. Stock solutions of different metal ions were prepared at a concentration of 1×10^{-3} M using double-distilled water. The specificity of the **AR-2** probe was evaluated in a DMSO solution. At an initial concentration of 2×10^{-5} M, the probe's selectivity towards various analytes, including cations at 1×10^{-3} M, was visually examined under UV light. No visible color change or peak shift was observed upon the addition of cationic analytes such as Ag^{+}, Ca^{2+}, Ce^{3+}, Co^{2+}, Cr^{3+}, Cr^{6+}, Er^{3+}, Fe^{2+}, Ga^{3+}, Gd^{3+}, Hg^{2+}, K^{+}, Li^{+}, Ln^{3+}, Mn^{3+}, Ni^{2+}, Pb^{2+}, Pr^{3+}, Sm^{3+}, Sr^{2+}, Tb^{3+}, Yb^{3+}, Yt^{3+}, and Zn^{2+}. In contrast, the fluorescence response of **AR-2** to Cu^{2+} and Fe^{3+} ions resulted in a noticeable color change, shifting from bright yellow to blue or pale yellow, which was discernible to the naked eye under a 365 nm UV lamp. No significant color change was observed for other analytes under either fluorescent or UV light (Fig. 2A). Both UV–visible and fluorescence spectrophotometers were employed to analyze the **AR-2** probe at a concentration of 2×10^{-5} M. The absorption spectra revealed two major peaks at 309 nm and 386 nm, while the emission spectra displayed peaks at 439 nm and 544 nm. The

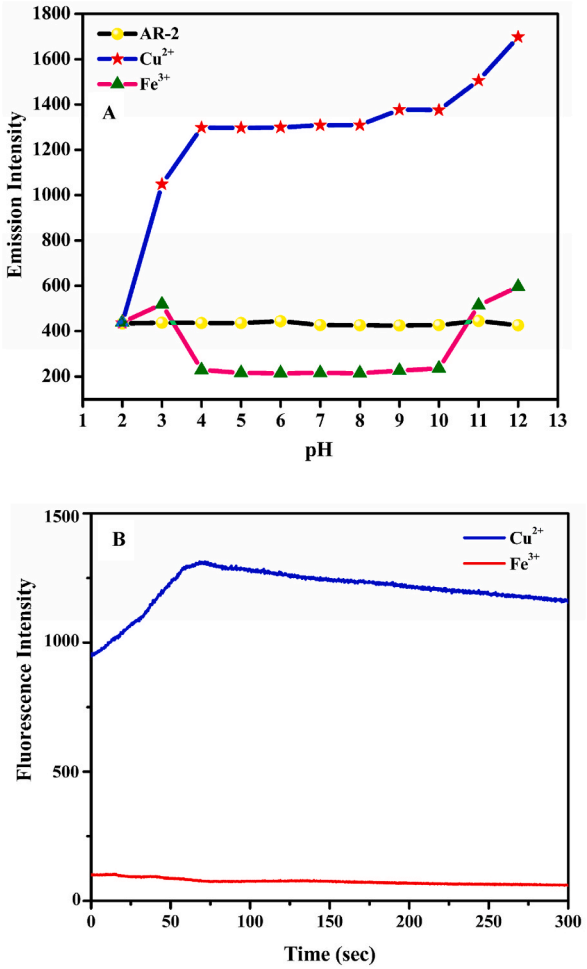

Fig. 5. (A) pH effect of **AR-2**/Cu^{2+}/Fe^{3+} and (B) Time response of **AR-2**/Cu^{2+} and **AR-2**/Fe^{3+}.

addition of Cu^{2+} and Fe^{3+} ions caused a significant blue shift in the emission spectra, whereas other cations did not produce noticeable changes. Analysis of the absorbance spectra showed notable shifts only for Cu^{2+}, Fe^{3+}, and Fe^{2+} ions (Fig. 2B). These fluorescence changes upon the addition of Cu^{2+} and Fe^{3+} suggest the formation of an **AR-2**-Cu^{2+}/Fe^{3+} complex, demonstrating the probe's excellent selectivity for Cu^{2+} and Fe^{3+} ions over other metal ions (Fig. 2C).

3.3. *Sensitivity of **AR-2**/Cu^{2+} and **AR-2**/Fe^{3+}*

In the fluorescence titration process, incremental amounts of Cu^{2+} and Fe^{3+} ions (10^{-3} M) were added to the **AR-2** probe, resulting in gradual changes in the emission band intensity. As depicted in Fig. S13A, the fluorescence intensity of **AR-2** at 450 nm increased steadily with rising Cu^{2+} concentration until it reached saturation at an **AR-2**/Cu^{2+} molar ratio of 1:1. This saturation suggests a 1:1 stoichiometry for the **AR-2**/Cu^{2+} complex, as confirmed by Job's plot in Fig. 3A. The notable increase in fluorescence intensity for **AR-2** was attributed to the formation of the chelating complex **AR-2**/Cu^{2+}, which inhibits the photoinduced electron transfer (PET) process. The fluorescence enhancement at 450 nm exhibited a strong linear correlation within the concentration range of 0–10 μM (R^2 = 0.97897), accompanied by distinct blue fluorescence emission (Fig. 4A). Using this linear relationship, the detection limit (LOD) was calculated to be 0.883×10^{-7} M, determined using 3σ/S. This LOD value exceeds the maximum acceptable Cu^{2+} limit set by the US EPA guidelines (20 μM) and surpasses most known sensors for Cu^{2+} [31,32].

The fluorescence intensity of **AR-2** (10 μM) at 455 nm decreased gradually with increasing Fe^{3+} concentration until reaching a 1:1 stoichiometry for the **AR-2**/Fe^{3+} complex, nearly completely quenching the fluorescence (Fig. S13B). This quenching indicates a 1:1 stoichiometry for the **AR-2**/Fe^{3+} complex, which is additionally confirmed by Job's plot (Fig. 3B). The notable fluorescence quenching is most likely due to the chelation-enhanced fluorescence quenching (CHEQ) effect of the paramagnetic Fe^{3+} ion. Furthermore, a strong linear correlation was found between the 455 nm fluorescence intensity and Fe^{3+} concentrations in the range of 0–10 μM (R^2 = 0.98305), with a detection limit of 1.05×10^{-7} M (Fig. 4B). This detection limit is significantly lower than the enforceable drinking water standard for Fe^{3+} set by the US EPA (5.4 μM) and is superior to those reported for other Fe^{3+} sensors in the literature [33,34]. In

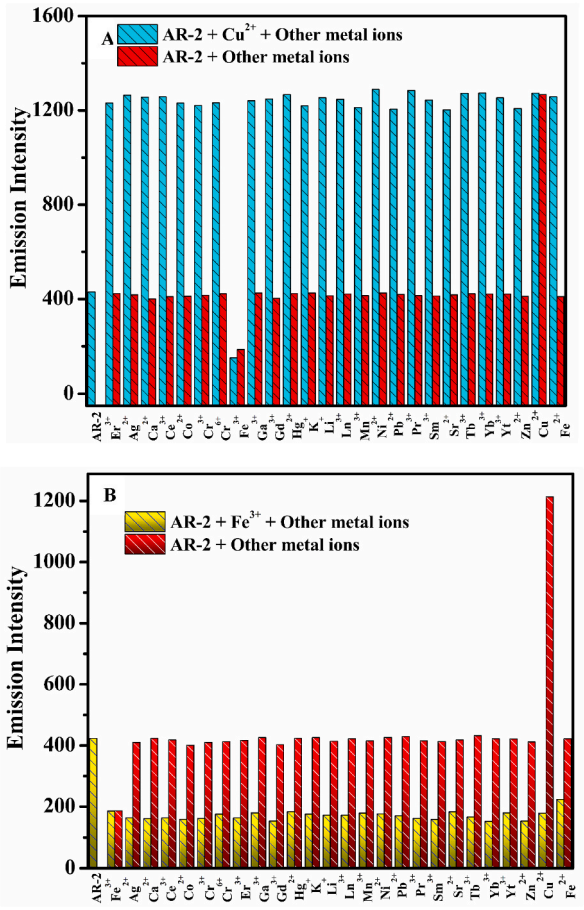

Fig. 6. (A) Interference studies of **AR-2**/Cu^{2+} and (B) Interference studies of **AR-2**/Fe^{3+}.

summary, these findings highlight the high sensitivity of the **AR-2** probe as an effective sensor for detecting Cu^{2+} and Fe^{3+} ions.

3.4. *pH studies of **AR-2** and **AR-2-Cu^{2+}/Fe^{3+}** and response time*

The fluorescence intensity of both the **AR-2** probe and the **AR-2**-Cu^{2+}/Fe^{3+} complex was evaluated across different pH levels, as shown in Fig. 5A. These results indicate that **AR-2** functions effectively as a fluorescent sensor for Cu^{2+}/Fe^{3+} ions within the pH range of 4–10, making it suitable for detecting these ions under physiological conditions. Notably, the **AR-2** probe also demonstrates effectiveness across a broader pH range of 2–12. Additionally, Fig. 5B illustrates that upon the addition of Cu^{2+}/Fe^{3+} ions to the **AR-2** solution, the interaction reaches equilibrium almost instantly. Within a minute, Cu^{2+}/Fe^{3+} ions can either enhance or quench the fluorescence of **AR-2**, eventually reaching saturation. This rapid responsiveness of **AR-2** to Cu^{2+} and Fe^{3+} ions highlights its potential as an efficient tool for real-time monitoring and detection of these ions.

3.5. *Interference studies*

Competitive tests were conducted to assess the practical efficacy of **AR-2**. As shown in both Fig. 6A and B, the fluorescence changes of **AR-2** induced by Cu^{2+}/Fe^{3+} remained largely unaffected even in the presence of various other metal ions. This indicates a strong preference of **AR-2** for Cu^{2+} and Fe^{3+} ions. The selectivity of **AR-2** for these ions compared to other paramagnetic metal ions may be attributed to the compatibility between **AR-2** and the size, charge, and electron configurations of the metal ions in their d and f orbitals. These findings suggest that **AR-2** exhibits robust resistance to interference, making it a promising fluorescent probe for detecting Cu^{2+} and Fe^{3+} ions.

Equation (1) can be used to determine the onset of the absorption peak by straight-line interpolation, which will yield the band gap. The band gap of the **AR-2** probe is smaller compared to the **AR-2**-Cu^{2+} and **AR-2**-Fe^{3+} complexes, as illustrated in Fig. S14.

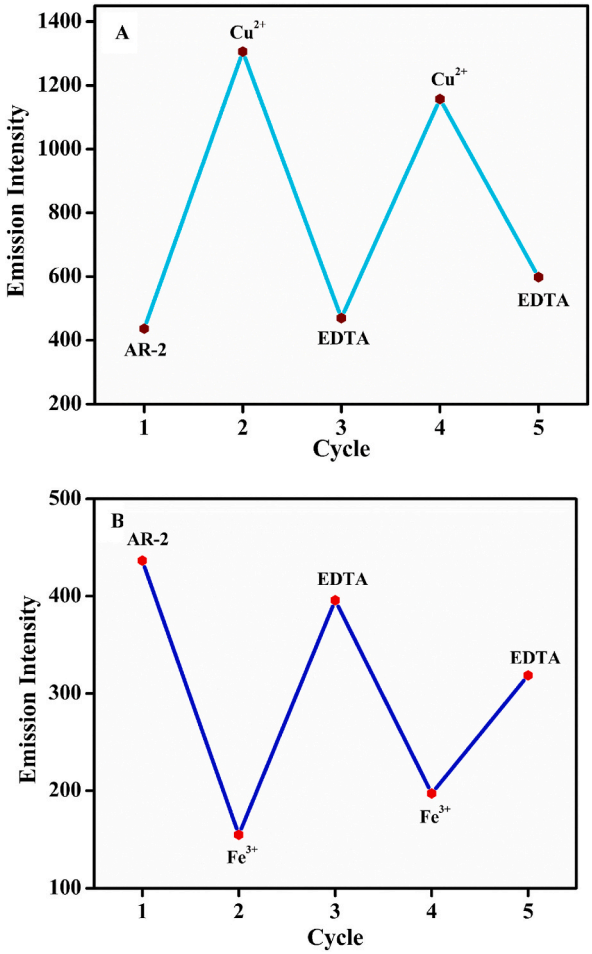

Fig. 7. (A) Reusability of **AR-2**/Cu^{2+} and (B) Reusability of **AR-2**/Fe^{3+}.

3.6. *Reversibility and reusability of probe **AR-2***

It is highly practical for a fluorescent sensor to be reversible and recyclable when detecting Cu^{2+}/Fe^{3+} ions. To test this capability with our **AR-2** probe, two rounds of systematic fluorescence titration tests with Cu^{2+}/Fe^{3+} ions, followed by the addition of EDTA, were conducted. As shown in Fig. S15, saturating **AR-2** with 1 equivalent of Cu^{2+} significantly enhanced fluorescence. Adding 1 equivalent of EDTA quenched the fluorescence, with near-complete recovery. Similarly, saturating **AR-2** with 1 equivalent of Fe^{3+} caused notable fluorescence quenching, which was almost fully restored by incubating with a saturated EDTA solution. This demonstrates that **AR-2**'s fluorescence intensity can be reversibly regulated by alternating the addition of Cu^{2+}/Fe^{3+} and EDTA, and **AR-2** can be reused for at least two cycles (Fig. 7A and B). These results suggest that **AR-2** exhibits excellent reversibility and regeneration for Cu^{2+}/Fe^{3+} detection, making it suitable for practical use.

3.7. *Binding mechanism*

By utilizing the Job's plot method, the binding ratio between the **AR-2** probe and Cu^{2+} and Fe^{3+} was assessed, revealing a 1:1 binding mode for both **AR-2**-Cu^{2+} and **AR-2**-Fe^{3+} complexes. Using the Benesi-Hildebrand (B-H) standard formula, where B-H=Intercept/Slope, binding constants of $0.9035 \times 10^3\ M^{-1}$ and $1.1179 \times 10^3\ M^{-1}$ were derived for Cu^{2+} and Fe^{3+}, respectively. The plot also demonstrated strong linearity, with correlation coefficients (R^2) of 0.9577 and 0.9907. These results suggest that the **AR-2** probe exhibits exceptional sensitivity to low concentrations of copper and iron cations, enabling precise detection even at trace levels (Fig. 8A and B).

To determine the binding mode between the **AR-2** probe and Cu^{2+}/Fe^{3+}, ^{1}H NMR titrations were conducted. Upon adding Cu^{2+}/Fe^{3+} ions (0–1 equivalent), the proton signals broadened due to the paramagnetic nature of the metal ions in the complex. Additionally, the chemical shift of the -NH_2 proton decreased and shifted slightly upfield (shielded), from 5.1 ppm to 5.0 ppm. However, no further spectral changes were observed beyond 0.50 equivalent of Cu^{2+}/Fe^{3+} ions, indicating the formation of a 1:1 **AR-2**/Cu^{2+}/Fe^{3+} complex

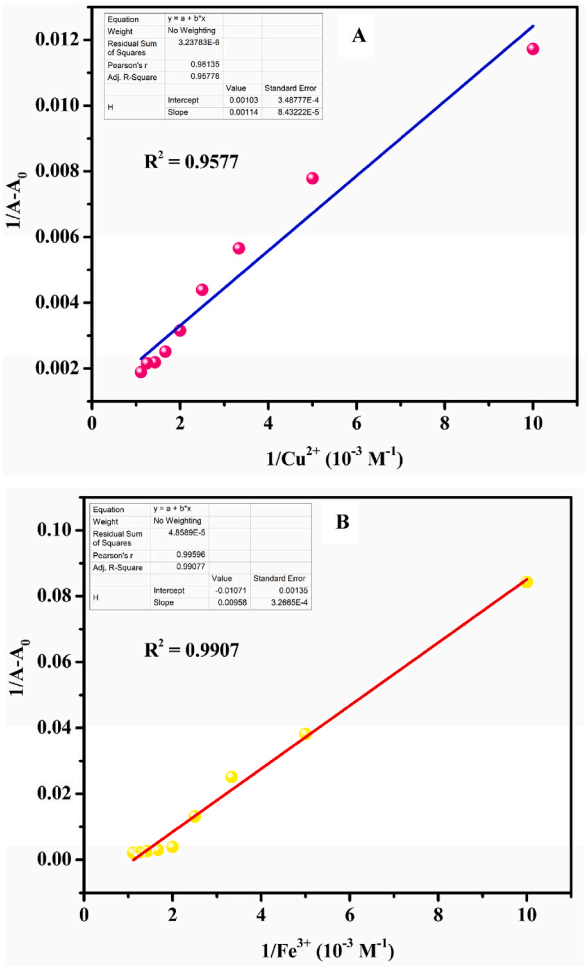

Fig. 8. (A) BH plot of **AR-2**/Cu^{2+} and (B) BH plot of **AR-2**/Fe^{3+}.

(Fig. 9). These shifts in chemical shift signals suggest coordination of the nitrogen atoms of the hydrazine unit with the Cu^{2+}/Fe^{3+} center, as supported by the ^{13}C NMR study. In the ^{13}C NMR spectrum of the **AR-2** probe, the thiol group attached to the imino carbon was initially observed at δ 162.28 ppm. Upon binding with Cu^{2+} ions, the hydrogen from the thiol group is removed, converting the sulfur to a sulfide ion. This results in the imino carbon becoming shielded, which shifts its signal to δ 155.09 ppm. This shift confirms the formation of a bi-coordinated complex between Cu^{2+} and **AR-2** through the thiol group, as illustrated in Figs. S16A and S16B. The binding mechanism was further confirmed through FT-IR analysis of the **AR-2**/Cu^{2+}/Fe^{3+} complex (Fig. S17). Initially, the **AR-2** probe shows stretching vibration bands at 3350 and 1627 cm^{-1} corresponding to the NH_2 and C=N groups, respectively, while the thiol group (-SH) peak appears around 2467 cm^{-1}. After complexation with Cu^{2+}/Fe^{3+}, the NH_2 stretching vibration band weakens, the C=N vibration band shifts to 1634 cm^{-1} and 1640 cm^{-1}, respectively, and the -SH peak disappears entirely at 2467 cm^{-1}. A new peak appears at 1578–1574 cm^{-1}, confirming the ring C-C stretching frequency in the **AR-2**-Cu^{2+}/Fe^{3+} complex. These changes further support the coordination of Cu^{2+}/Fe^{3+} with the **AR-2** probe.

Additional confirmation was provided using Electrospray Ionization Mass Spectrometry (ESI-MS), where the measured mass for **AR-2**/Cu^{2+}/Fe^{3+} closely matched the expected mass: for **AR-2**-Cu^{2+}, the calculated mass was *m/z* 600.1483 and the observed mass was *m/z* 601.1561 (M + H); for **AR-2**-Fe^{3+}, the calculated mass was *m/z* 593.1531. observed mass: *m/z* 593.1590 (M^+) (Figs. S18A and S18B).

The proposed binding mechanism of the **AR-2** probe for Cu^{2+}/Fe^{3+} is outlined in Scheme 2. In the Photoinduced Electron Transfer (PET) mechanism, electrons are transferred from donor atoms, such as sulfur (S) and nitrogen (N) in the **AR-2** molecule, to the excited state of the fluorophore. This electron transfer results in a redistribution of electron density away from the fluorophore, which diminishes its fluorescence emission. As a result, the energy available for light emission is reduced, leading to weak or negligible fluorescence. When **AR-2** interacts with Cu^{2+} ions, the electron transfer from the donor atoms to the fluorophore is hindered. Consequently, the fluorophore's ability to emit light is less disrupted, resulting in a significant increase in fluorescence. This enhancement in fluorescence is known as the Chemically Enhanced Fluorescence (CHEF) effect. Conversely, in the presence of Fe^{3+} ions, fluorescence quenching occurs due to the Ligand-to-Metal Charge Transfer (LMCT) effect. Here, electron density is transferred

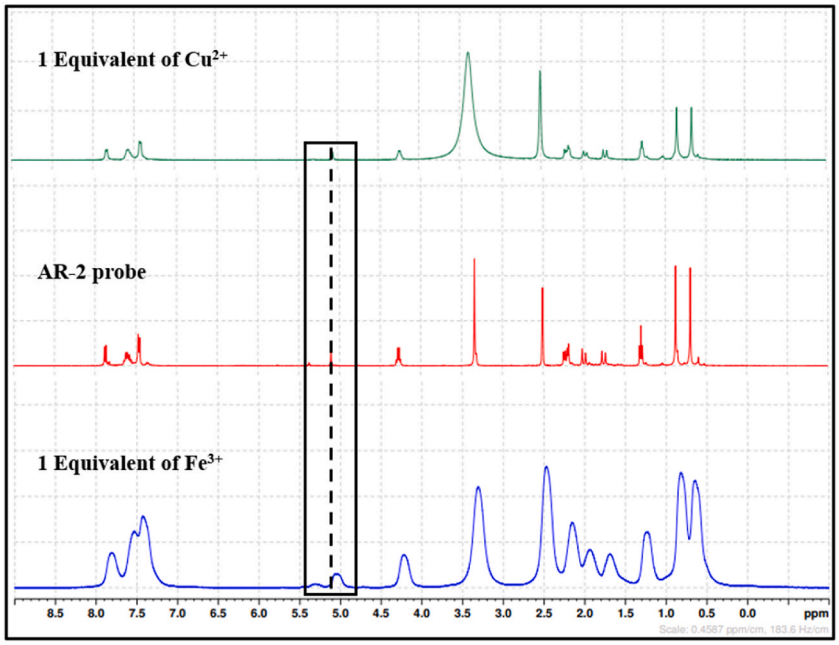

Fig. 9. ^{1}H NMR spectra of **AR-2**/Cu^{2+}/Fe^{3+} complex.

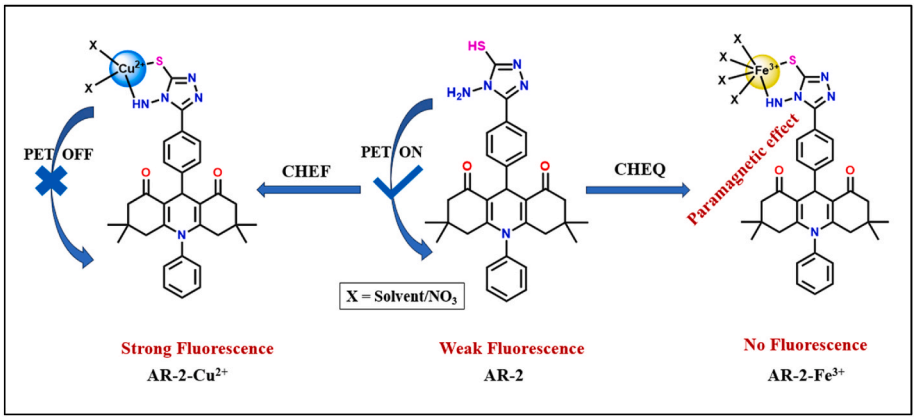

Scheme 2. The proposed sensing mechanism of **AR-2** and Cu^{2+}/Fe^{3+} ion.

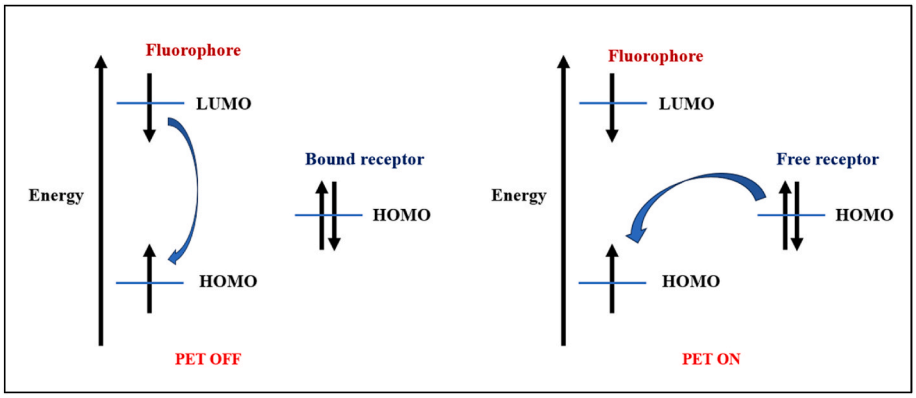

Fig. 10. The general energy level diagram of Fluorophore.

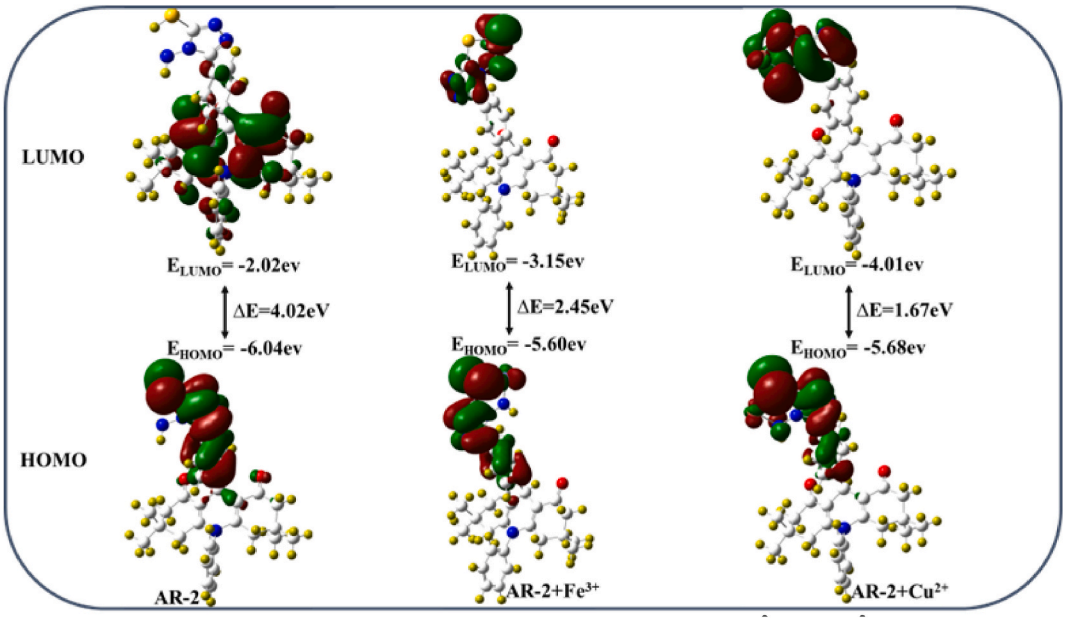

Fig. 11. The energy level diagram of the probe **AR-2** with Cu^{2+} and Fe^{3+} ions.

from the **AR-2** ligand to the Fe^{3+} ion. The Fe^{3+} ion, with its unpaired d electrons and paramagnetic nature, effectively quenches fluorescence. The transfer of electrons from the excited states of **AR-2** to the d-orbitals of Fe^{3+} ions reduces light emission, leading to a marked decrease in fluorescence. This phenomenon is referred to as the Chemically Quenched (CHEQ) effect (Fig. 10).

3.8. Computational study

The probe **AR-2** forms a chelate with Cu^{2+}/Fe^{3+} ions through interactions involving the -SH and amine nitrogen groups. Structural, electronic, and optical properties were analyzed using B3LYP/6-31G (d,p) Gaussian 09 software. Fig. 11 illustrates the HOMO and LUMO of **AR-2** and its Cu^{2+}/Fe^{3+} complexes. The energy gap between the HOMO and LUMO for **AR-2** is 4.02 eV, which decreases significantly upon complex formation with Cu^{2+}/Fe^{3+} ions. The **AR-2**-Cu^{2+} complex exhibits a HOMO-LUMO energy difference of 1.67 eV, while the **AR-2**-Fe^{3+} complex displays 2.45 eV, indicating a strong interaction between **AR-2** and Cu^{2+}/Fe^{3+} cations. In these complexes, the thiol and amine substituted groups in **AR-2** act as the HOMO, while the electrons are distributed across the acridinedione base moiety at the LUMO.

Chelation of Cu^{2+} with **AR-2** not only hinders the PET process in the chemosensor but also enhances the molecule's rigidity by restricting free rotation, resulting in a chelation-induced enhanced fluorescence (CHEF) effect. These findings demonstrate the "turn-on" mode of our probe towards Cu^{2+}. Conversely, the fluorescence "turn-off" phenomenon of **AR-2** upon binding with Fe^{3+} is attributed to the lower energy of the HOMO in the **AR-2**-Fe^{3+} complex compared to **AR-2**, which acts as an electron acceptor. Moreover, the LUMO of the complex is lower than that of **AR-2**, facilitating electron acceptance from **AR-2** and leading to fluorescence quenching via the PET mechanism.

3.9. Hands-on application

3.9.1. Paper strips, swab test, and real samples

The effectiveness of **AR-2** in selectively responding to copper and iron ions was practically evaluated using test strips and swab test techniques (Figs. S19A and S19B). Comparisons between probe **AR-2** and previously reported sensors are provided in Table S1. Additionally, real-time analysis of water samples and food samples for **AR-2**/Cu^{2+}/Fe^{3+} are detailed in Tables S2 and S3, respectively.

3.9.2. Fluorescence images of red chori and black chickpea sprouts

To monitor the uptake of Cu^{2+} and Fe^{3+} in plants and assess the suitability of **AR-2**, red chori and black chickpea sprouts were cultivated for 24 h at an appropriate temperature, as shown in Fig. 12A. The experimental protocol involved fluorescence visualization to track the uptake of Cu^{2+} and Fe^{3+} in the sprouts and examine the fluorescence imaging process (Fig. 12B). After incubation with the **AR-2** probe, the sprouts displayed yellow fluorescence for the **AR-2** probe, blue fluorescence for Cu^{2+}, and no fluorescence for Fe^{3+} under UV light (365 nm) (Fig. 12C). Subsequent treatment with EDTA caused the fluorescence signal to disappear, indicating the probe's absorption by the sprouts, interaction with Cu^{2+} to produce blue fluorescence, and the removal of Cu^{2+} by EDTA. These results suggest that **AR-2** is effective for detecting Cu^{2+} and Fe^{3+} in sprouts.

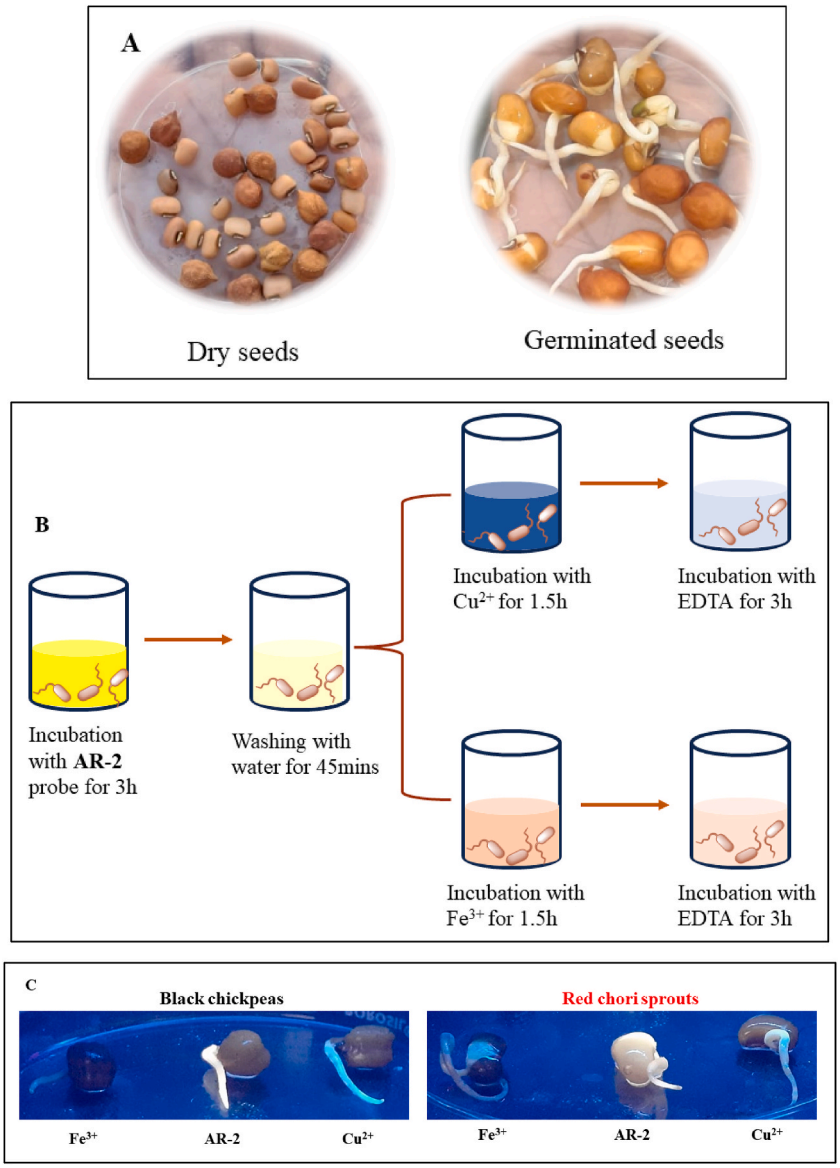

Fig. 12. (A) Growth of sprouts from red chori and black chickpeas, (B) Schematic diagram of the experimental design for fluorescence imaging in sprouts and (C) Fluorescence imaging of sprouting the solution of **AR-2**/Cu^{2+}/Fe^{3+}.

*3.9.3. **AR-2** as a fingerprint sensor*

Fluorescent chemical compounds designed to visualize latent fingerprints have become widely used in forensic investigations. Due to its enhanced stability and distinct fluorescence properties, the **AR-2** sensor was employed for fingerprint visualization. The process is illustrated graphically in Fig. 13A. After preparing the **AR-2** solution, it was used to view fingerprints on a TLC plate under a UV lamp (365 nm). The resulting dark yellow glow was captured in the image. When solutions of Cu^{2+} and Fe^{3+} ions were fingerprinted onto the **AR-2**-coated slide, Cu^{2+} ions caused a fluorescence "turn-on" effect, while Fe^{3+} ions caused a fluorescence "turn-off" effect (Fig. 13B).

4. Conclusion

In conclusion, this study introduces **AR-2**, a cost-effective fluorescent sensor based on a triazole-substituted acridinedione derivative, designed for the rapid and simultaneous detection of Cu^{2+} and Fe^{3+} ions. The sensor's remarkable sensitivity and selectivity have been demonstrated through extensive spectroscopic analyses and computational investigations, elucidating its structural features, photophysical properties, and sensing mechanism. **AR-2** exhibits a "turn-on" response to Cu^{2+} ions and a "turn-off" response to Fe^{3+} ions, with fast reversibility and response times, indicating its potential for environmental monitoring and analytical chemistry applications. Its broad pH range and low detection limits further enhance its practical applicability for real-world sensing. Validation

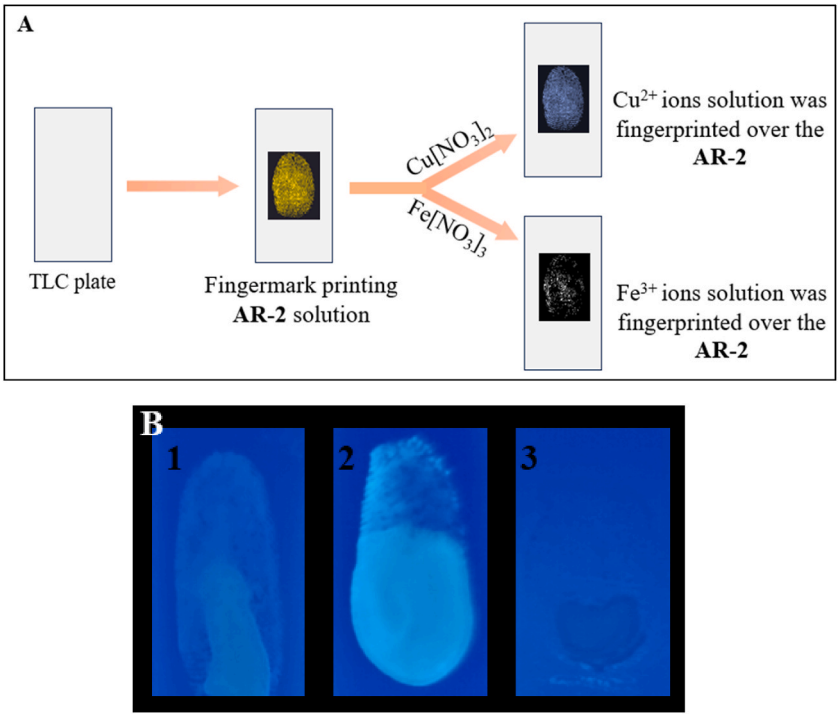

Fig. 13. (A) Diagram illustrating the creation of a fingerprint using an **AR-2** molecule optimized with metal ions and (B) The visual image of **AR-2** and **AR-2**/Cu^{2+}/Fe^{3+} under UV light (365 nm) (1. The prepared **AR-2** solution was fingerprinted on the TLC plate, 2. Cu^{2+} ions solution was fingerprinted over the **AR-2** and 3. Fe^{3+} ions solution was fingerprinted over the **AR-2**.).

experiments including paper test strips, swab tests, fingerprint studies, sprout tests, and analyses of water and food samples confirm the sensor's efficacy and versatility. Overall, **AR-2** proves to be a promising tool for the simultaneous detection of Cu^{2+} and Fe^{3+} ions, with significant implications for future research and practical applications in analytical chemistry and environmental monitoring.

Data availability

Information will be provided upon request.

Funding

No funding.

CRediT authorship contribution statement

Srinivasan Parthiban Ragavi: Writing – original draft, Investigation, Formal analysis. **Dhakshanamurthy Thirumalai:** Writing – review & editing, Validation, Data curation. **Indira Viswambaran Asharani:** Writing – review & editing, Project administration, Funding acquisition, Conceptualization. **Vidya Radhakrishnan:** Validation. **Peter Jerome:** Formal analysis.

Declaration of competing interest

The authors declare that they have no known competing financial interests or personal relationships that could have appeared to influence the work reported in this paper.

Acknowledgement

We are grateful for the laboratory and sophisticated instrumentation facility (SIF) provided by the Vellore Institute of Technology. We extend special thanks to Dr. K. Sathyanarayanan, Professor in the Department of Chemistry and School of Advanced Sciences and Enbanathan Saravanan, for their invaluable support and assistance with the DFT study.

Appendix A. Supplementary data

Supplementary data to this article can be found online at https://doi.org/10.1016/j.heliyon.2024.e38318.

References

[1] H. Tang, M. Xu, F. Shi, G. Ye, C. Lv, J. Luo, L. Zhao, Y. Li, Effects and mechanism of nano-copper exposure on hepatic cytochrome P450 enzymes in rats, Int. J. Mol. Sci. 19 (2018) 2140–2156.
[2] M. Sharifi-Rad, N.V. Anil Kumar, P. Zucca, E.M. Varoni, L. Dini, E. Panzarini, J. Rajkovic, P.V. Tsouh Fokou, E. Azzini, I. Peluso, A. Prakash Mishra, Lifestyle, oxidative stress, and antioxidants: back and forth in the pathophysiology of chronic diseases, Front. Physiol. 11 (2020) 694.
[3] C. Vulpe, B. Levinson, S. Whitney, S. Packman, J. Gitschier, Isolation of a candidate gene for Menkes disease and evidence that it encodes a copper–transporting ATPase, Nat. Genet. 3 (1) (1993) 7–13.
[4] P.C. Bull, G.R. Thomas, J.M. Rommens, J.R. Forbes, D.W. Cox, The Wilson disease gene is a putative copper transporting P-type ATPase similar to the Menkes gene, Nat. Genet. 5 (4) (1993) 327–337.
[5] Y.H. Hung, A.I. Bush, R.A. Cherny, Copper in the brain and Alzheimer's disease, J. Biol. Inorg Chem. 15 (2010) 61–76.
[6] M. Bisaglia, L. Bubacco, Copper ions and Parkinson's disease: why is homeostasis so relevant? Biomolecules 10 (2) (2020) 195.
[7] G. Manfredi, Z. Xu, Mitochondrial dysfunction and its role in motor neuron degeneration in ALS, Mitochondrion 5 (2) (2005) 77–87.
[8] L. Guo, T. Tang, L. Hu, M. Yang, X. Chen, Fluorescence assay of Fe(III) in human serum samples based on pH dependent silver nanoclusters, Sensor. Actuator. B Chem. 241 (2017) 773–778.
[9] J. Wang, D. Zhang, Y. Liu, P. Ding, C. Wang, Y. Ye, Y. Zhao, A N-stablization rhodamine-based fluorescent chemosensor for Fe^{3+} in aqueous solution and its application in bioimaging, Sensor. Actuator. B Chem. 191 (2014) 344–350.
[10] R.R. Crichton, D.T. Dexter, R.J. Ward, Metal based neurodegenerative diseases from molecular mechanisms to therapeutic strategies, Coord. Chem. Rev. 252 (2008) 1189–1199.
[11] R.S. Britton, K.L. Leicester, B.R. Bacon, Iron toxicity and chelation therapy, Int. J. Hematol. 76 (2002) 219–228.
[12] F. Mejía-Rodríguez, T. Shamah-Levy, S. Villalpando, A. García-Guerra, I. Méndez-Gómez Humarán, Iron, zinc, copper and magnesium deficiencies in Mexican adults from the National Health and Nutrition Survey 2006, Salud Publica Mex. 55 (2013) 275–284.
[13] S. Şahan, U. Şahin, Determination of copper (II) using atomic absorption spectrometry and Eriochrome blue black R loaded Amberlite XAD-1180 resin. Clean: Soil, Air, Water 38 (5-6) (2010) 485–491.
[14] P. Wainwright, D. Wadey, P. Cook, An inductively coupled plasma mass spectrometry method for relative free copper determination and generation of a pediatric reference interval, Ann. Clin. Biochem. 55 (4) (2018) 485–490.
[15] A.R. Date, Y.Y. Cheung, M.E. Stuart, J. Xiu-Hua, Application of inductively coupled plasma mass spectrometry to the analysis of iron ores, J. Anal. At. Spectrom. 3 (5) (1988) 653–658.
[16] B. Yan, P.J. Worsfold, Determination of cobalt(II), copper(II) and iron(II) by ion chromatography with chemiluminescence detection, Anal. Chim. Acta 236 (1990) 287–292.
[17] P. Gahlyan, R. Bawa, H. Jain, M. Dalela, A. Joshi, C.N. Ramachandran, A.K. Prasad, A. Kaur, R. Kumar, Isatin-triazole-functionalized rhodamine: a dual sensor for Cu^{2+} and Fe^{3+} ions and its application to cell imaging, ChemistrySelect 4 (2019) 7532–7540.
[18] Y. Yuan, S. Sun, S. Liu, X. Song, X. Peng, Highly sensitive and selective turn-on fluorescent probes for Cu^{2+} based on rhodamine B, J. Mater. Chem. B 3 (2015) 5261–5265.
[19] H. Fang, P. Huang, F. Wu, A novel jointly colorimetric and fluorescent sensor for Cu^{2+} recognition and its complex for sensing S^{2-} by a Cu^{2+} displacement approach in aqueous media, Spectrochim. Acta 204 (2018) 568–575.
[20] S. Zhang, Q. Niu, L. Lan, Novel oligothiophene-phenylamine based Schiff base as a fluorescent chemosensor for the dual-channel detection of Hg^{2+} and Cu^{2+} with high sensitivity and selectivity, Sensor. Actuator. B Chem. 240 (2017) 793–800.
[21] O. Oter, K. Ertekin, C. Kirilmis, M. Koca, M. Ahmedzade, Characterization of a newly synthesized fluorescent benzofuran derivative and usage as a selective fiber optic sensor for Fe(III), Sensor. Actuator. B Chem. 122 (2007) 450–456.
[22] L.J. Fan, W.E. Jones, A highly selective and sensitive inorganic/organic hybrid polymer fluorescence "turn-on" chemosensory system for iron cations, J. Am. Chem. Soc. 128 (2006) 6784–6785.
[23] C. Li, J. Liu, S. Alonso, F. Li, Y. Zhang, Upconversion nanoparticles for sensitive and in-depth detection of Cu^{2+} ions, Nanoscale 4 (2012) 6065–6071.
[24] M. Yu, M. Shi, Z. Chen, F. Li, X. Li, Y. Gao, J. Xu, H. Yang, Z. Zhou, T. Yi, C. Huang, Highly sensitive and fast responsive fluorescence turn-on chemodosimeter for Cu^{2+} and its application in live cell imaging, Chem. Eur J. 14 (2008) 6892–6900.
[25] J. Wang, T. Wei, F. Ma, T. Li, Q. Niu, A novel fluorescent and colorimetric dual-channel sensor for the fast, reversible and simultaneous detection of Fe^{3+} and Cu^{2+} based on terthiophene derivative with high sensitivity and selectivity, J. Photochem. Photobiol., A Chemistry. 383 (2019) 111982.
[26] M.H. Lee, T.V. Giap, S.H. Kim, L.Y.H. Lee, C. Kang, J.S. Kim, A novel strategy to selectively detect Fe(III) in aqueous media driven by hydrolysis of a rhodamine 6G Schiff base, Chem. Commun. 46 (2010) 1407–1409.
[27] G.Y. Gao, W.J. Qu, B.B. Shi, P. Zhang, Q. Lin, H. Yao, W.L. Yang, Y.M. Zhang, T.B. Wei, A highly selective fluorescent chemosensor for iron ion based on 1H-imidazo [4,5-b] phenazine derivative, Spectrochim. Acta 121 (2014) 514–519.
[28] M. Wang, J. Wang, W. Xue, A. Wu, A benzimidazole-based ratiometric fluorescent sensor for Cr^{3+} and Fe^{3+} in aqueous solution, Dyes Pigments 97 (2013) 475–480.
[29] Y. Liang, R. Wang, G. Liu, S. Pu, Bifunctional Cu^{2+}/Fe^{3+} probe with independent signal outputs based on a photochromic diarylethene with a dansylhydrazine unit, ACS Omega 4 (2019) 6597–6606.
[30] G. Harichandran, P. Parameswari, P. Shanmugam, Synthesis and photophysical properties of functionalized fluorescent 4H-chromenes and benzo[a] chromenophenazines as Fe^{3+} and Cu^{2+} ion sensor, Sensor. Actuator. B Chem. 272 (2018) 252–263.
[31] E. Şenkuytu, A high selective "Turn-Off" aminopyrene based cyclotriphosphazene fluorescent chemosensors for Fe^{3+}/Cu^{2+} ions, Inorg. Chim. Acta. 479 (2018) 58–65.
[32] P. Thordarson, Determining association constants from titration experiments in supramolecular chemistry, Chem. Soc. Rev. 40 (2011) 1305–1323.
[33] B. Zhang, H. Liu, F. Wu, G. Hao, Y. Chen, C. Tan, Y. Tan, Y. Jiang, A dual-response quinoline-based fluorescent sensor for the detection of Copper (II) and Iron (III) ions in aqueous medium, Sensor. Actuator. B Chem. 243 (2017) 765–774.
[34] P.R. Sahoo, S. Kumar, Photochromic spirooxazine as a highly sensitive and selective probe for optical detection of Fe^{3+} in aqueous solution, Sensor. Actuator. B Chem. 226 (2016) 548–552.